THE SARAF CW 40 MEV PROTON/DEUTERON ACCELERATOR

I. Mardor, D. Berkovits, I. Gertz, A. Grin, S. Halfon, G. Lempert, A. Nagler, A. Perry, J. Rodnizki, L. Weissman, Soreq NRC, Yavne, Israel
K. Dunkel, M. Pekeler, C. Piel, P. vom Stein, RI Research Instruments GmbH, Bergisch Gladbach, Germany

Abstract

The Soreq Applied Research Accelerator Facility, SARAF, is currently under construction at Soreq NRC. SARAF is based on a continuous wave (CW), proton/deuteron RF superconducting linear accelerator with variable energy (5–40 MeV) and current (0.04-2 mA). Phase I of SARAF consists of a 20 keV/u ECR ion source, a low energy beam transport section, a 4-rod RFQ, a medium energy (1.5 MeV/u) transport section, a superconducting module housing 6 half-wave resonators and 3 superconducting solenoids, a diagnostic plate and a beam dump. Phase II will include 5 additional superconducting modules. The RFQ is in routine operation with protons since 2008 and has been further operated with molecular hydrogen and deuterons at low duty cycle. RF conditioning of the RFQ to enable deuteron CW acceleration is on going. The RF fields and dynamic cryogenic losses of the superconducting module have been measured with a VCO and the phase and amplitude stability at high fields has been measured with the SARAF LLRF system. Furthermore, proton and deuteron beams have been accelerated through the superconducting module. These were the first ever ion beams to be accelerated through half-wave resonators. Recent SARAF Phase I commissioning results are presented.

SARAF OVERVIEW

SARAF is currently under construction at Soreq NRC [1]. It will consist of a medium energy (up to 40 MeV) high current (up to 2 mA, CW, upgradeable to 4 mA) RF superconducting linac of protons and deuterons, beam lines and a target hall with several irradiation stations. A schematic layout of the facility is given in Fig. 1. Details on its required parameters and a technical description of its components are given in [2].

Due to the technical novelty in the accelerator, the project has been divided to two phases. Phase I includes the ECR ion source, the RFQ, a prototype superconducting module (PSM), a diagnostic plate (D-Plate) and a beam dump (See Fig. 2). Phase I further includes the design of the full accelerator (based on beam dynamics simulations [3]) and the design and risk reduction of foreseen applications. Phase II includes construction of rest of the accelerator and its applications.

This paper present recent commissioning results of SARAF Phase I. A brief summary of the RFQ conditioning effort is given. The emphasis is on the PSM and on beam operation results of both protons and deuterons.

PHASE I COMMISSIONING

The SARAF accelerator is designed, manufactured, installed and commissioned by RI Research Instruments GmbH [4], in collaboration with Soreq NRC personnel.

Phase I is fully installed on site. The ECR source is routinely operated. Details on its construction and commissioning can be found in [5]. The RFQ and PSM are still under intense commissioning, which is described in the following sub-sections. In parallel to commissioning each of the components, beam operation with both protons and deuterons through the RFQ and the PSM has been demonstrated and is described in detail below.

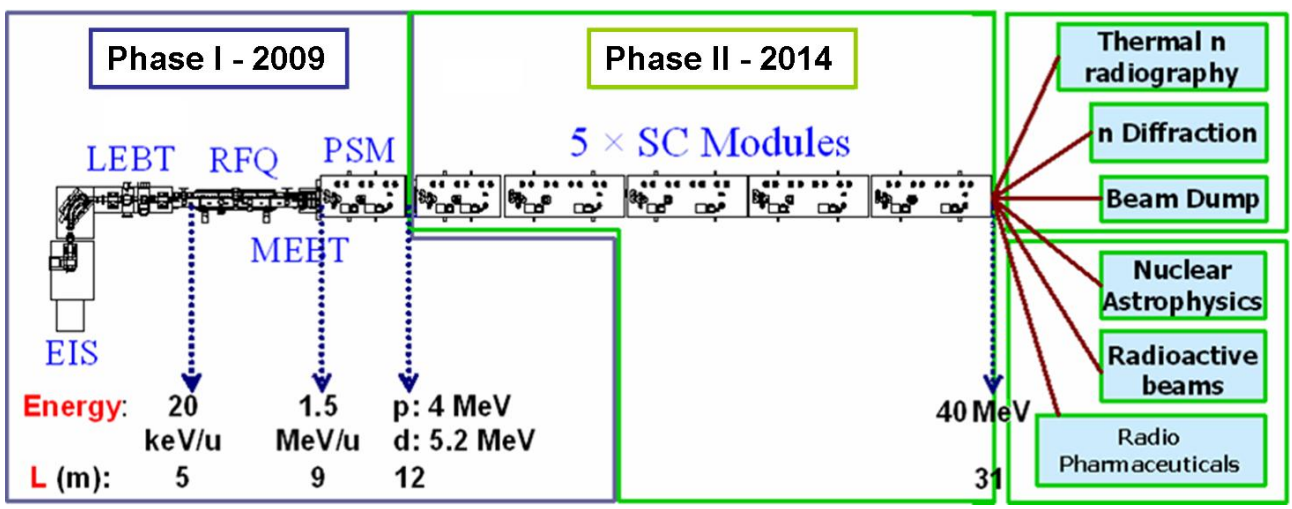

Figure 1: Schematic layout of SARAF. The PSM includes 6 β=0.09 HWR cavities. The first Phase II SC module includes has the same lattice. The latter 4 modules each include 8 β=0.15 HWR cavities.

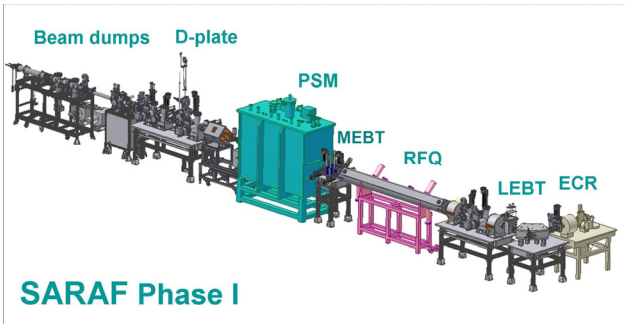

Figure 2: Schematic view of SARAF Phase I.

RFQ

The SARAF RFQ is a 176 MHz 4-rod CW RFQ [6]. The main challenge in this RFQ is removing 250 kW from its ~3.8 meter rods, an unprecedented heat density.

The RFQ commissioning is comprised of two processes which are being executed in parallel: RF conditioning up to 65 kV, the voltage that is required for deuteron acceleration and beam commissioning, mainly with protons that require half of the deuteron field.

The RF conditioning effort is ongoing for the last three years. Work up to September 2008 yielded unstable results, which enabled deuteron operation with a duty cycle not higher than 15% [7].

During February 2009 the RFQ rods were dismantled and re-machined in order to circumvent extensive field emission between the bottom part of the rods and the stems of the opposite voltage rods. Following two months of conditioning, it was possible to reach the nominal deuterons power, 260 kW, with a duty cycle of 80% for periods of up to 30 minutes [8].

The latter conditioning campaign ended when one RF blade of one of the RFQ tuning plates melted. This plate was replaced, but a different RF blade melted. When the RFQ was opened to replace the tuning plate, it was discovered that the low energy plunger partially melted as well (See Fig. 3).

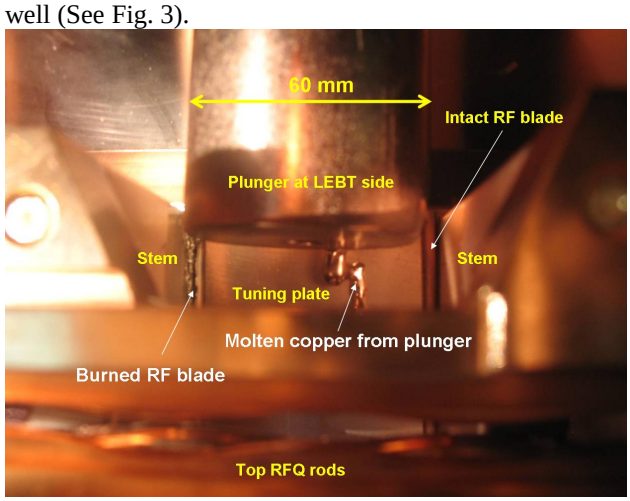

Figure 3: View of the open RFQ from above the rods. Note the melted plunger tip and the burned RF blade in the tuning plate's left side.

In parallel, it became evident during conditioning that above 200 kW, the RFQ end plates' temperatures are continuously rising and RF trips occur before they reach thermal equilibrium.

The above results prompted an intensive, detailed, 3D finite element simulation of RF fields and surface currents and the subsequent heat loads in several RFQ regions. This effort resulted in new designs for the tuning plates, end plates and plungers. Details of the simulations and new design are beyond the scope of this paper and will be presented in another publication. The new components were installed in the RFQ in August 2009 and currently it is under conditioning.

Although the SARAF RFQ is still not performing up to its design goals, its recent upgrade emphasized a main advantage of the 4-Rod RFQ, namely the relative simplicity of opening it and replacing its components.

PROTOTYPE SUPERCONDUCTING MODULE (PSM)

The PSM includes six 176 MHz, β=0.09 half wave resonators (HWR) made of bulk Nb and three 6 T superconducting solenoids inserted amongst them. A drawing of the PSM is given in Fig. 4.

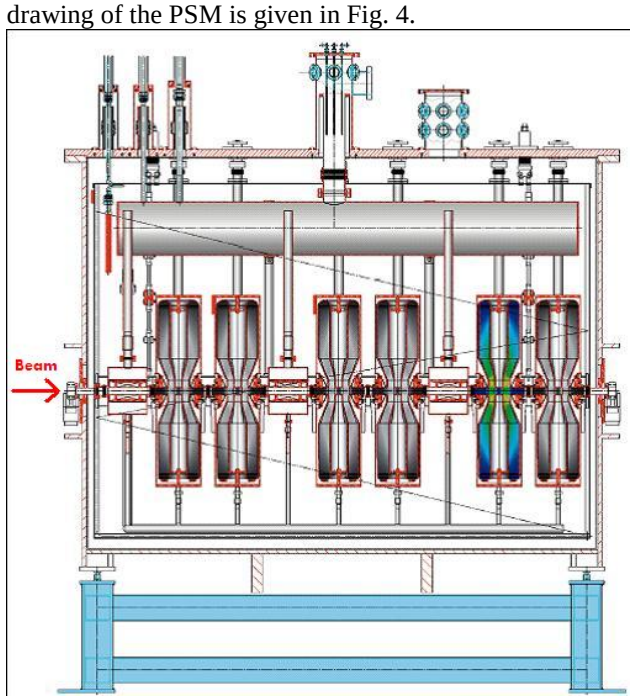

Figure 4: The SARAF PSM, containing 6 SC HWRs (β=0.09) and 3 SC solenoids (reproduced from [9]). Beam height is 1400 mm above floor.

Details of the PSM manufacturing, design parameters and cavity vertical cold tests are described in Ref. 9.

The results of the first acceleration of protons through the PSM, with only the first three cavities, were presented in Ref. 8. Recent RF commissioning of the PSM and preliminary beam operation results are given in Ref. 10.

In the following we describe in more detail recent beam operation through the PSM. A deuteron beam has been passed through a detuned PSM and a proton beam was

accelerated by all 6 cavities working in parallel under the control of the SARAF LLRF system [11].

Deuteron beam operation

A deuteron beam has been passed through a detuned PSM in order to measure the needed RFQ power for deuteron operation and to check the alignment of all Phase I components (Fig. 2).

The deuteron beam was with a low duty cycle of 10^{-4} (100 μsec pulses at a frequency of 1 Hz). The instantaneous current at the LEBT was 4.6 mA. The RFQ power was administered at a duty cycle of 10%, to ensure continuous operation at and above the expected nominal power. We measured the summed signal of the two MEBT BPMs, the beam current at the D-Plate Faraday Cup and the beam energy by extracting Time-of-Flight from the two D-Plate phase probes, which are 1.2 m apart. Details of Phase I beam diagnostics are given in Ref. 12.

The results for beam energy and current measurements at the D-Plate and MEBT are given in Figures 5 and 6.

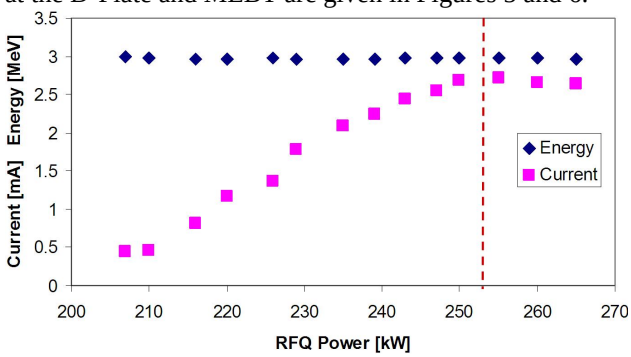

Figure 5: Deuteron beam energy and instantaneous current at the D-Plate, following acceleration at the RFQ and drift through the detuned PSM. The dashed red line marks the deduced optimal RFQ power.

Fig. 5 shows that the beam reaches its nominal energy of 3 MeV at an RFQ power lower than the value needed to reach maximum transmission. This has been observed also for proton beams [13] and is consistent with beam dynamics simulations [14].

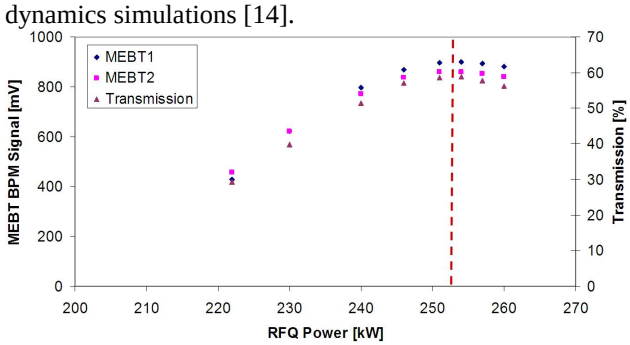

Figure 6: Deuteron MEBT BPMs signals and transmission through RFQ+PSM, from the D-Plate Faraday Cup current divided by the LEBT current. The dashed red line marks the deduced optimal RFQ power.

Fig. 6 shows that the maximum transmission is approximately 59%. Quantitative comparison between transmission through the RFQ and the PSM is not possible at this point, since the MEBT BPMs are not calibrated to provide a beam current measurement. However, the similarity of the patterns indicates that the beam transmission is dictated by the RFQ. This result is lower than the previously reported value of 70% [7], probably because the beam current and emittance at the RFQ entrance were lower at the previous run, as discussed in the proton beam transmission sub-section.

The results of Figs. 5 and 6 indicate that the nominal RFQ power for deuteron operation should be 252-253 kW. This value includes beam (approximately 7 kW in this case). This value is slightly higher than 4 times the nominal RFQ power for protons, which was recently measured to be 58 kW. The source of this increase is not clear yet, since recent comparisons between the RFQ voltage and the input power show no significant losses due to dark current. Notice that the nominal power for protons was reduced with respect to the value given in Ref. 13, due to the re-machining of the RFQ rods [8].

Fig. 7 shows deuteron beam transverse profiles at the D-Plate, as a function of the RFQ power duty cycle.

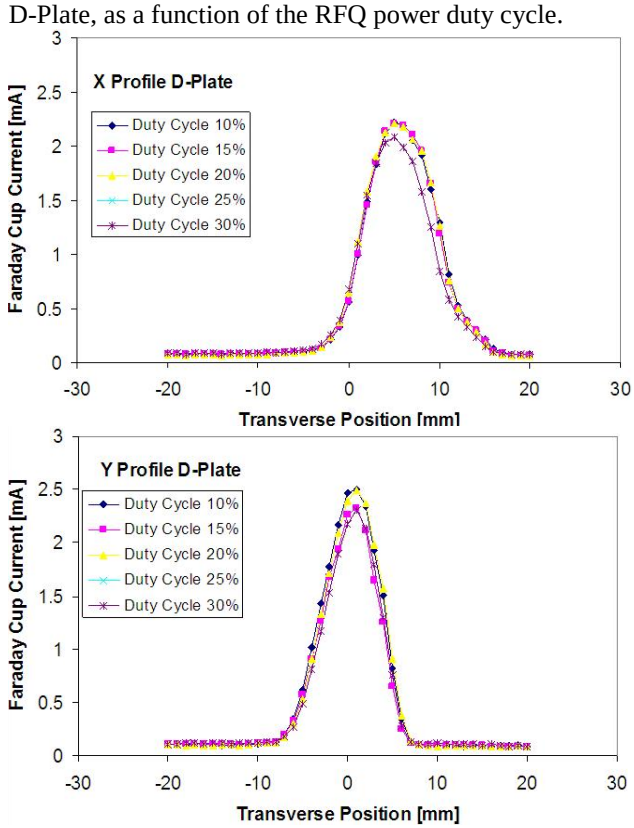

Figure 7: Transverse beam profiles of the deuteron beam, when accelerated by the RFQ and passed through the detuned PSM. Profiles are given for several RFQ power duty cycles. Top: Horizontal. Bottom: Vertical.

It can be seen that the X profile is slightly wider and off center by approximately 5 mm, whereas the Y profile is sharper and centered. The Y profile was centered by adjusting the field in the quadrupole situated between the PSM and the D-Plate, whereas the X profile was less sensitive to this device. This indicates that the beam

entered that quadrupole off its axis in the Y plane. The steerers down stream of the PSM were not used.

Fig. 7 further shows that up to a duty cycle of 30% In the RFQ power, there is hardly an effect on the beam profile, which indicates that there are no significant thermal movements of the rods in the average power range of 26 through 78 kW.

Proton Beam Operation

A proton beam at a duty cycle of 10^{-4} has been accelerated through the PSM with all six cavities in operation, up to energy of 3.7 MeV. The RFQ power was CW. Stable operation was limited to 15-20 minutes, mostly due to instabilities induced by cavities 4 and 5.

The accelerator parameters were set based on beam dynamics simulations using the code TRACK [15]. Due to the distance of about 1 meter between the RFQ exit and the first PSM cavity, the latter must be used as a buncher. Bunching takes place as the beam drifts through the second cavity and acceleration starts only at the third one. This is clearly demonstrated by beam dynamics simulations [3]. The PSM cavities voltages and synchronous phases that were used in the 3.7 MeV protons run are given in Table 1.

Table 1: Accelerating voltages and synchronous phases for the 3.7 MeV proton beam run. The corresponding Epeak and Eacc are given for reference.

Cavity	Acceleration voltage [kV]	Epeak [MV/m]	Eacc [MV/m]	Synchronous Phase [deg]
1	150	4.5	0.9	-95
2	85	2.6	0.5	0
3	700	21.0	4.3	0
4	550	16.5	3.4	-20
5	550	16.5	3.4	-20
6	900	27.0	5.6	-20

The values of Eacc were extracted from the acceleration voltage by using the acceleration length $Lacc=(n\_gap/2)\cdot\beta\cdot\lambda$, where $\beta=0.094$ and $\lambda=1.70$ m for the PSM's 176 MHz cavities.

Tuning the PSM cavities was performed by rotating the phase at low accelerating voltage (usually around 150 – 200 kV), finding the phase where the beam energy is maximal, and then setting the phase to the synchronous value that is given in Table 1. An example of a cavity tuning in this run is given in Ref. 10.

The beam energy increase along the PSM is given in Fig. 8. These beam energy measurements were performed via the Time-of-Flight method, using two phase probes at the D-Plate. In addition, the simulated energy values after each cavity are given, and good agreement is obtained.

The above run was repeated in the following day and the results were consistent with the original one. In this run, beam energy was measured also via Rutherford scattering off a gold foil, using the SARAF beam halo monitor [16]. The Rutherford scattering and ToF results were consistent, as can be seen in Ref. 10.

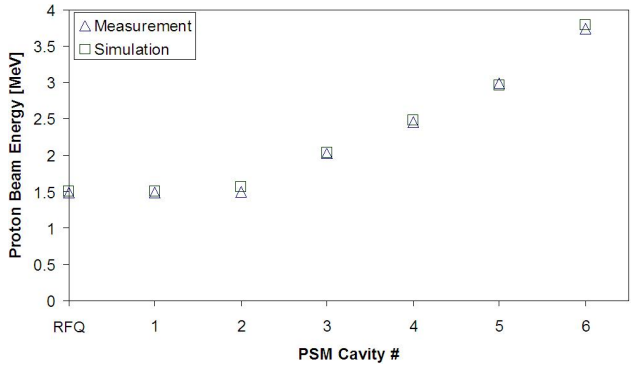

Figure 8: Proton beam energy increase along the PSM cavities. RFQ exit energy is included. Measurement results are consistent with bean dynamic simulations.

As mentioned above, stable operation with six cavities was not possible continuously for more than 15-20 minutes. By that time, one of the cavities, usually 4 or 5 will have tripped. The recovery time was several minutes, but this prevented beam emittance measurements.

A possible explanation of the observed instabilities might be insufficient processing of cavities 4 and 5. Operation at medium acceleration voltage of these cavities might cause significant changes in the power load of the cryoplant, which in turn cause liquid Helium pressure variations that trip the cavities. To avoid this problem in general, the cavities' heaters are controlled by the LLRF, to ensure that the total (heater + RF) power from each cavity is constant. This level was set to 9 W per cavity in this run. Fig. 9 shows the cryoplant trends during the six cavity run and during the run with cavities 4 and 5 detuned. A clear correlation between the stability of cryoplant power (depicted by the LHe inlet valve opening trend) and that of PSM operation is observed.

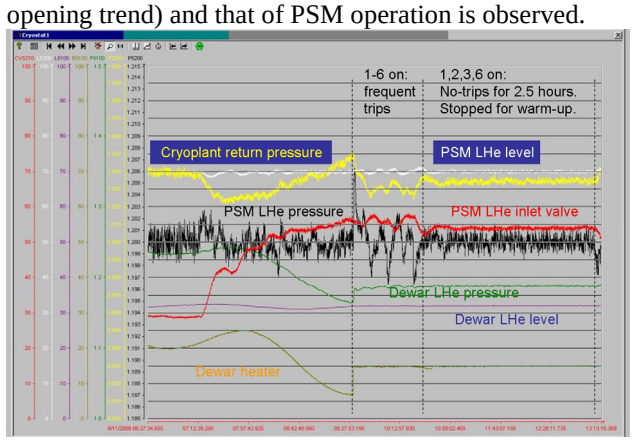

Figure 9: Cryoplant trends during the proton beam runs with six and four cavities. As long as the cryoplant power (PSM LHe inlet valve opening) is unstable, numerous trips occur. Stable power is related to excellent pressure stability (< ±1.5 mbar) and continuous operation.

Based on Ref. 10, it is possible that cavity 4 generated much more than 9 W while in operation, but cavity 5 seemed to produce lower power. Subsequent tests of the LLRF modules exhibited frequent spikes in module #5, which might have caused some of the observed trips.

Proton Beam Transmission

For the run described above, the proton beam transmission from the LEBT to the D-Plate was only 42% (2.1 mA instantaneous current at the D-Plate, with respect to 5.0 mA at LEBT), significantly lower than the abovementioned deuteron value (59%) and the previously reported proton value (60%) [8]. Based on Fig. 6, this is due solely to the RFQ. Subsequent proton runs at lower instantaneous current exhibit higher transmission, up to approximately 70% at 2.1 mA. An RFQ transmission increase at reduced current was previously observed [7]. Since the LEBT deuteron emittance is better than for protons, and the LEBT proton emittance at 2.0 mA is better than at 5.0 mA [7], it is probable that the transmission reduction is due to increased LEBT emittance.

Nevertheless, since the previous proton result was recorded before re-machining the RFQ rods, we investigated whether the re-machined rods might reduce the transmission. The RFQ electric field has been originally tuned with tuning plates that altered the cells' resonance frequency and relative field value. This resulted in a generally uniform field with variations of 5% peak to peak [6]. When the rods were re-machined [8], the cells' capacitance was significantly reduced. In order to re-tune the RFQ, tuning plates had to be lowered or even removed. Unfortunately, the overall effect was not enough. The rods themselves were slightly shifted to increase the capacitance, but all in all, the field uniformity was significantly reduced, as can be seen in Fig. 10.

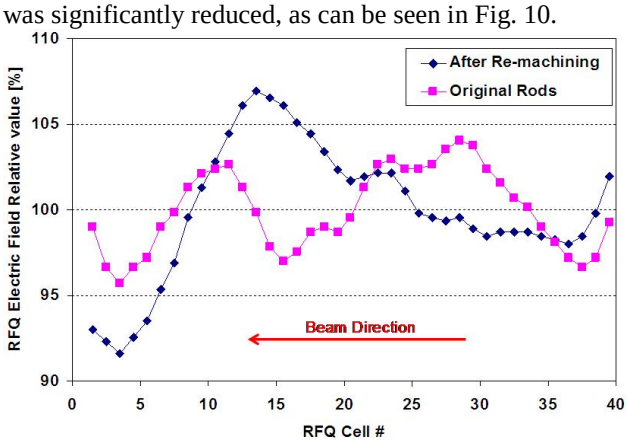

Figure 10: RFQ relative electric field profile before and after the rods re-machining. The large variation at the RFQ downstream side might be a partial cause of the decreased beam transmission.

Beam dynamics simulations using the above two RFQ field distributions are given in Fig. 11. It is seen that the existing distribution reduces beam transmission by less than 5%. The additional beam loss is in the high energy part of the RFQ. This is consistent with Ref. 6, where a simulated field decrease of 70% in part of the RFQ causes a decrease of 15% in transmission.

In conclusion, although the existing RFQ field distribution might account for some of the transmission reduction, there are probably additional causes. One should note that the given beam dynamics results are for a perfectly aligned beam, entering the RFQ with transverse emittance of 0.2 π·mm·mrad. Slight relative misalignment between the LEBT and the RFQ and a larger LEBT emittance might increase the non-uniform field effect.

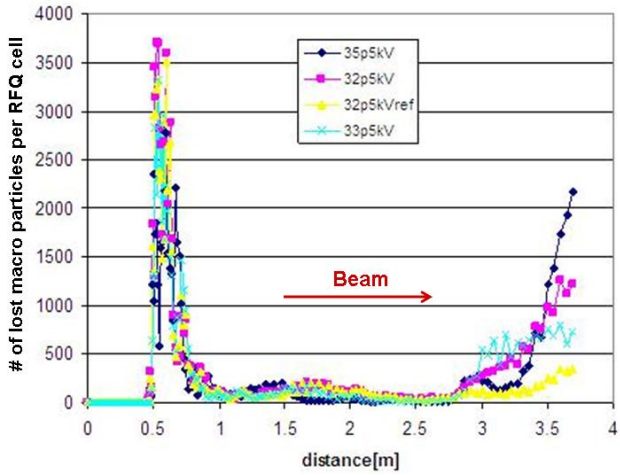

Figure 11: Simulated beam loss along the RFQ based on the original field profile (yellow) and the existing field profile (pink). The light and dark blue profiles are for the existing profile with a voltage higher by 1 and 3 kV, respectively. Each macro particle corresponds to 8 nA of actual beam.

Longitudinal Emittance of Protons

In order to obtain quantitative measurements of the accelerated proton beam, we detuned cavities 4 and 5, and with the remaining cavities were able to run continuously for several hours. We set cavities 1-3 to the values of Table 1, cavity 6 to 400 kV, and varied the phase of cavity 6. For this variation, the beam energy and its energetic width are plotted in Fig. 12.

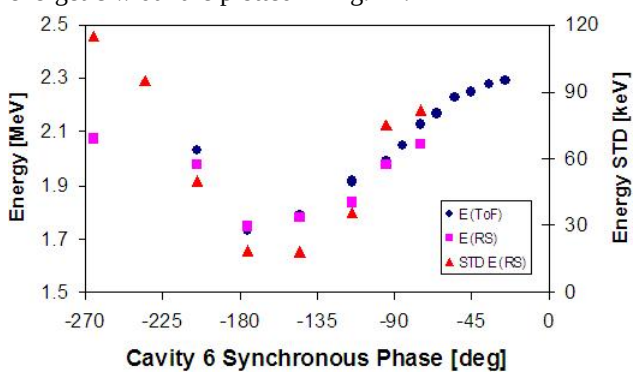

Figure 12: Proton beam energy and energetic width at the D-Plate, as a function of cavity 6 synchronous phase. Cavities 4 and 5 are detuned. Beam energy was measured by both ToF and Rutherford Scattering (RS). Energetic standard deviation (STD) was measured by RS. STD values include the detector's and target's contributions.

These energy and energetic width values were used to extract the longitudinal emittance of the proton beam at the exit of cavity 3. Notice that usually, the "measuring cavity" (cavity 6) is set to a bunching phase of -90

degrees, its voltage is varied, which in turn changes the energetic width without changing the beam energy, and the bunch length is measured for each setting [17 and references therein]. In our case, the voltage was constant and the phase was changed, varying both the beam's energy and energetic width, as shown in Fig. 12.

The beam longitudinal transfer is described by a drift transfer matrix from the exit of cavity 3 to cavity 6, an acceleration element with energy gain Uacc through cavity 6 and another drift element from cavity 6 to the D-Plate. Algebraically, the phase and energetic widths at the D-Plate ($\Delta\Phi_x$, ΔE_x) are generated from the cavity 3 variables ($\Delta\Phi_e$, ΔE_e) by:

$$\begin{bmatrix}\Delta\Phi_x\\ \Delta E_x\end{bmatrix} = R*\begin{bmatrix}\Delta\Phi_e\\ \Delta E_e\end{bmatrix};\quad R=\begin{bmatrix}1 & Y_2\\ 0 & 1\end{bmatrix}\begin{bmatrix}1 & 0\\ X_1 & 1\end{bmatrix}\begin{bmatrix}1 & Y_1\\ 0 & 1\end{bmatrix} \quad (1)$$

where X_1 and Y_i are given by:

$$X_1 = Uacc\ * \sin(\phi / 360\ * 2\pi) * 2\pi / 360$$
$$Y_i = 1/(mc^3\gamma_i^3\beta_i^3) * 360\ / T * D_i$$

where ϕ is the synchronous acceleration phase, T is the beam period (T=1/f, f=176 MHz), m is the proton mass and D_i are the relevant drift distances.

The beam matrix σ_x at the D-Plate is given by:

$$\begin{bmatrix}\sigma_{55x} & \sigma_{56x}\\ \sigma_{65x} & \sigma_{66x}\end{bmatrix} = R*\begin{bmatrix}\sigma_{55e} & \sigma_{56e}\\ \sigma_{65e} & \sigma_{66e}\end{bmatrix}R_T$$

where the matrix R is defined in Eq. 1 and σ_e is the beam matrix at cavity 3. While in Ref. 17 longitudinal emittance is extracted from the bunch length (σ_{55}), here it emerges from the energetic width (σ_{66}). Further algebraic development of the algorithm is beyond the scope of this paper and is presented elsewhere [18]. Based on it, the energy variance at the D-Plate is given by:

$$\sigma_{66x}(X_1) = (\sigma_{55e} + 2Y_1\sigma_{56e} + Y_1^2\sigma_{66e})X_1^2 + 2(\sigma_{56e} + Y_1\sigma_{66e})X_1 + \sigma_{66e} \quad (2)$$

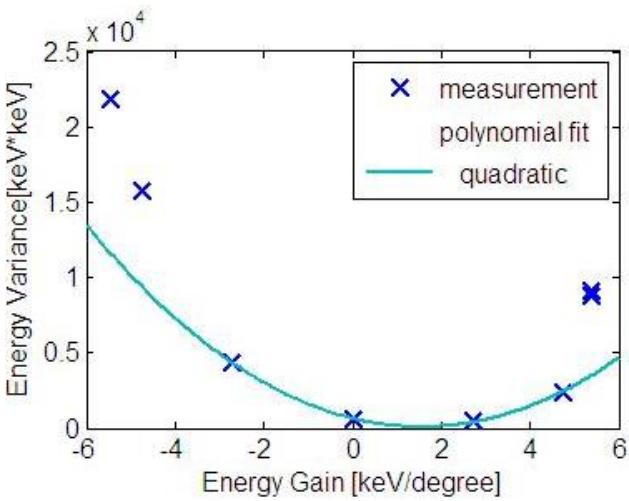

Figure 13: Energy variance at cavity 6 (Eq. 2) versus the energy gain per degree in this cavity. A polynomial fit is valid in only part of the energy gain range.

The basic assumptions in the algorithm are that all cavities effects on the beam are linear and the effect of space charge is negligible. A metric of the validity of these assumptions in our measurement is the fit of the energy variance $\sigma_{66x}(X_1)$ to a second order polynomial in the variable X_1 (see Eq. 2). A plot of the measured energy variance versus X_1, the energy gain per degree, and its fit to a second order polynomial, is given in Fig. 13. One can see that a polynomial fit is valid only in a certain range of the energy gain per degree. This may imply that the PSM setup for this proton run was not optimal and non-linear effects were eminent, or it may be a space charge effect.

Indeed, fitting the energy variance to a polynomial in the valid range dictated by Fig. 13, generates a rms longitudinal emittance of 120±5 π·deg·keV/u at the exit of cavity 3. This value is higher than the RFQ exit result (30 π·deg·keV/u), measured using the D-Plate Fast Faraday Cup (FFC) and reported in Ref. 7.

This emittance growth is a result of the phase setup, in which the phase of cavity 3 was set to 0, and cavities 4 and 5 were detuned. It may also be a result of the change in the RFQ field uniformity (Fig. 10) between the two measurements. Future emittance measurements will be taken with a more linear setup.

Transverse Emittance of Protons

The transverse emittance was measured by a slit and wire system, which is part of the D-Plate, and is described in Ref. 12. This measurement was taken with cavities 1-3 at the setup of Table 1 and cavities 4-6 detuned. The energy at the exit of cavity 3 was 2.02 MeV (See Fig. 8). The raw data was analyzed by the code SCUBEEx [19]. The X-X' projection of the transverse phase space and the transverse emittance values are given in Fig. 14.

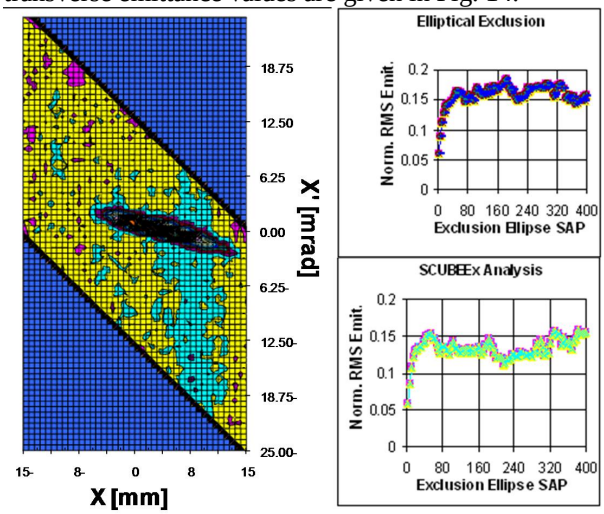

Figure 14: Left: X-X' projection of the transverse phase space of the proton beam with cavities 1-3 set to the parameters of Table 1 and cavities 4-6 detuned. The plot was generated by SCUBEEx. Right: Emittance values calculated via SCUBEEx [18].

Notice that the X-X' plot in Fig. 14 includes the beam ellipse (dark blue) and a satellite distribution (light blue),

which source is not yet clear. The r.m.s. normalized transverse emittance was extracted by both SCUBEEx and an internal Soreq algorithm [20], where in both methods it was attempted to exclude the effect of the satellite distribution.

The combined result of the two algorithms is 0.l4±0.02 π·mm·mrad. This value is significantly lower than the previously reported result at the RFQ exit (with the same measuring apparatus and a similar LEBT setup) [7]. This may be due to the very low RFQ transmission (42%, as reported above), which might be cutting off a significant amount of the beam's phase space.

SUMMARY AND OUTLOOK

The commissioning of Phase I of SARAF is on-going and is approaching finalization. The current challenges include conditioning the RFQ to enable acceleration of CW deuteron beams and optimizing the PSM to reach the proton and deuteron beam target values.

Several RFQ internal parts have been re-designed and installed. This effort should enable CW deuteron operation.

Low duty cycle 2.7 and 2.1 mA deuteron and proton beams have been accelerated through SARAF Phase I, up to energies of 3.0 and 3.7 MeV. For deuterons, the PSM cavities were detuned. For protons, all 6 cavities were operated in medium and high field and provided acceleration consistent with the predictions of beam dynamics simulations.

Finalization of protons and deuterons beam commissioning through the entire Phase I is foreseen for the end of 2009.

REFERENCES

[1] http://www.soreq.gov.il/default_EN.asp

[2] A. Nagler et al., “Status of the SARAF Project”, LINAC'06, Knoxville, August 2006, MOP054, p. 168 (2006).

[3] J. Rodnizki et el., "Lattice Beam Dynamics Study at Low β For SARAF/EURISOL Driver 40/60 MeV 4 mA d&p Superconducting Linac", HB2008, Knoxville, August 2008, WGB15 (2008).

[4] http://www.research-instruments.de. A former Accel Instruments GmbH activity.

[5] K. Dunkel et al., "Performance of the SARAF Ion Source", PAC'07, Alboquerque, June 2007, TUPAN009, p. 1407 (2007).

[6] P. Fischer et al., "Tuning a CW 4-Rod RFQ", LINAC'06, Knoxville, August 2006, THP064, p. 728 (2006).

[7] A. Nagler et al., "The SARAF CW 40 MeV Proton/Deuteron Accelerator", LINAC'08, Victoria, September 2008, MO203 (2008).

[8] I. Mardor et al., "The Status of the SARAF CW 40 MeV Proton/Deuteron Accelerator", PAC'09, Vancouver, May 2009, FR5REP087 (2009).

[9] M. Pekeler et al., “Development of a Superconducting RF Module for Acceleration of Protons and Deuterons at Very Low Energy”, LINAC'06, Knoxville, August 2006, TUP034, p. 321 (2006).

[10] A. Perry et al., "SARAF Superconducting Module Commissioning Status", SRF'09, Berlin, September 2009, TUPPO029, (2009).

[11] M. Pekeler et al., "Development of Low Level RF Control Systems for Superconducting Heavy Ion Linear Accelerators, Electron Synchrotrons and Storage Rings", PAC'05, Knoxville, May 2005, WPAT068, p. 1 (2005).

[12] C. Piel et al., "Beam Operation of the SARAF Light Ion Injector", PAC'07, Albuquerque, June 2007, TUPAN011, p. 1410 (2007).

[13] C. Piel et al., "Phase 1 Commissioning Status of the 40 MeV Proton/Deuteron Accelerator SARAF", EPAC'08, Geona, June 2008, THPP038, p. 3452 (2008).

[14] J. Rodnizki at al., "Beam Dynamics Simulation of the 1.5 MeV Proton Beam Measured at the SARAF RFQ Exit", EPAC'08, Genoa, June 2008, THPP041, p. 3458 (2008).

[15] P. N. Ostroumov et al., "TRACK", ANL, March 27, 2006.

[16] L. Weissman et al., "First Experience at SARAF with Proton Beams using the Rutherford Scattering Monitor", DIPAC'09, Basel, May 2009, TUPB20 (2009).

[17] A. V. Feschenko et al., "The First Results of Bunch Shape Measurements in the SNS Linac", LINAC'04, Lubeck, August 2004, TUP63, p. 408 (2004).

[18] J. Rodnizki, Internal Soreq Report, 2009.

[19] M. P. Stockly et al., "Self-Consistent, unbiased root-mean-square emittance analysis", Rev. Sci. Inst. 75, 1646 (2004).

[20] S. Halfon, Internal Soreq Report, 2009.